JOURNAL OF MATERIALS SCIENCE 16 (1981) 159–169

Microstructural study of ε-iron–carbonitrides formed by a glow discharge technique

D. GERARDIN, J. P. MORNIROLI, H. MICHEL, M. GANTOIS
Laboratoire de Genie Metallurgique, Ecole des Mines, Parc de Saurupt, 54 042 Nancy Cedex, France

The microstructure and phase transformations occurring in ϵ-iron–carbonitrides have been studied by means of X-ray and electron diffraction, electron microscopy and Mössbauer spectrometry. Ordering of the interstitial atoms, N or C, results in a hexagonal unit cell for $Fe_3(C, N)$ with parameters $a' = a\sqrt{3}$ and $c' = c$ where a and c are the lattice parameters of the hexagonal close-packed (h c p) iron unit cell. Stacking faults on $(0\,0\,0\,1)_\epsilon$ planes and partial dislocations with Burgers vector $\mathbf{b} = \frac{1}{3}\langle 1\,0\,\bar{1}\,0\rangle$ are observed in quenched ϵ-$Fe_4(C, N)$. After quench-aging, the carbonitrides show a structural hardening due to the precipitation of a metastable phase. Slow cooling of ϵ-carbonitrides with less than 25 at % interstitials leads to the precipitation of γ'-carbonitride and ferrite in ϵ-phase grains which allows the orientation relationships between the ϵ-, γ'- and α-phases to be defined and a model of the ϵ-phase–γ'-phase transformation to be proposed.

1. Introduction

The use of cheap materials under conditions of severe mechanical stress has led to many new developments of surface thermochemical treatments. The present work examines the use of nitriding and carbonitriding treatments in a glow discharge at low temperatures to study the microstructure of ϵ iron–carbonitrides.

The basic principle of these treatments is the electrical dissociation of gases which allows the two main parameters – the temperature and the activity of the gas mixture – to be varied independently. Thus, many configurations of nitrided and carbonitrided layers can be formed on pure iron and steels. More particularly, single-phase layers of ϵ- or γ'-iron–carbon nitrides which have good resistance to abrasion and wear can be obtained. A better knowledge of phase transformations and plastic deformation mechanisms allows the treatment conditions to be adjusted in order to maximize the mechanical properties of the surface.

The present paper is concerned with a microstructural study of ϵ-iron–carbonitride with two compositions close to $Fe_4(C, N)$ and $Fe_3(C, N)$ in pure iron foils and ARMCO iron bulk specimens. Ordering of the interstitial atoms is examined in an ϵ-iron–carbonitride with the stoichiometric formula $Fe_3(C_{0.32}N_{0.68})$. The phase transformations occuring during cooling or quench-aging, together with the type of stacking defects present, are also studied in the ϵ-carbonitride $Fe_{3.85}(C_{0.18}N_{0.82})$.

2. Experimental procedure

The samples were carbonitrided by ion bombardment, the main features of which have already been described by several authors [1–3]. The composition of the carbonitrides obtained by this process is dependent on the nitrogen, hydrogen and methane partial pressures of the treatment atmosphere, the nature of the sample, the temperature and the duration of the treatment.

Two kinds of pure iron samples were carbonitrided:

(a) Foils of electrolytic iron, remelted in a vacuum and rolled to 10–40 μm thickness (see Table I). They were fully transformed to ϵ-iron–carbonitride after ion carbonitriding for several hours at a temperature of 640° C. These foils have a constant interstitial content throughout since thermodynamic equilibrium between the gas

0022–2461/81/010159–11$03.10/0

TABLE I Composition of the iron samples

Sample	Content (wt%)				
	C	Mn	Si	P	S
Electrolytical iron foils	0.015	0.06	0.03	0.024	0.014
ARMCO iron bulk specimens	0.01	< 0.01	< 0.01	0.005	0.001

atmosphere and the solid is achieved. The structure of these foils was observed by electron microscopy using a Philips EM 300 electron microscope. Thin foils for electron microscopy were obtained by electro-polishing in a 5% perchloric acid and 95% ethylene glycol monobutilic ether solution at 5° C and with a d.c. voltage of 17 V.

(b) Bulk samples of ARMCO iron (see Table I) with parallelepiped shape (10 mm × 15 mm × 20 mm) were carbonitrided between 570 and 580° C in a well-defined reactive atmosphere. A single phase ϵ-layer was superficially formed, followed by the nitrogen diffusion layer in ferrite; these two layers were sometimes separated by a thin austenite film. These configurations are similar to those obtained on steels by gas or molten salt nitriding or carbonitriding processes usually used in industrial treatments. As these layers are diffusionally formed, they show gradients in carbon and nitrogen contents. To study the structure, thin foils were obtained from different depths by mechanically polishing the specimens from both surfaces to within 20 μm of the required levels and finally ultra-thinning by ion bombardment. X-ray experiments were performed with a THETA 60 CGR diffractometer using $CoK\alpha_1$ radiation. Samples for optical microscopy were etched with a 4% nital solution.

The nitrogen content of the homogeneous foils was analysed by the micro-Kjeldahl method, and the carbon content was analysed by coulometry. The glow discharge optical spectrometry technique allows the carbon and nitrogen profiles to be determined in bulk samples [4].

3. Experimental results

Between the 550° C and 700° C isotherms of the Fe–C–N ternary phase diagram, a large equilibrium domain of the hexagonal ϵ-iron–carbonitride exists. The solubility of carbon atoms is important in this phase and can reach 3 wt % at the treatment temperature which is usually chosen near 570° C. The iron atoms occupy a close-packed hexagonal lattice (h c p), with a and c parameters which vary with interstitial concentration. Hence, they vary, respectively, from 2.667 to 2.764 Å and from 4.349 to 4.420 Å when the concentration rises from 20 to 33 at% [5]. The carbon and nitrogen atoms occupy some of the six octahedral interstitial sites of the h c p lattice. These sites form a hexagonal sub-lattice with parameters a and $c/2$.

3.1. ϵ-$Fe_3(C, N)$ carbonitride

X-ray and electron diffraction patterns of carbonitrides with compositions near $Fe_3(C, N)$ show extra-reflections caused by ordering of interstitial atoms in the octahedral vacancies (Fig. 1). These extra-reflections can be interpreted using a new hexagonal unit cell (labelled $\epsilon_{a\sqrt{3}}$ in the present paper) with parameters $a' = a\sqrt{3}$ and $c' = c$ which give fundamental reflections $(h\,k\,i\,l)$ for $h - k = 3m$, where m is an integer, and superlattice reflections for other values. These latter reflections have intensities dependent only on the atomic scattering factors of carbon and nitrogen.

Interstitial atom order has already been observed in ϵ-nitrides by Jack [5] and Hendricks and Kostings [6]. These authors describe hexagonal superlattices with $a' = a\sqrt{3}$ and $c' = c$ for Fe_3N and Fe_2N and with $a'' = 2a\sqrt{3}$ and $c'' = c$ for $Fe_{24}N_{10}$ and $Fe_{24}N_6$.

3.1.1. Antiphase boundaries

Observation of antiphase boundaries in thin foils is of particular interest as it confirms the order of interstitial atoms (Fig. 2). In the case of the ϵ-iron–carbonitride, with the particular composition $Fe_3(C, N)$, only two octahedral interstices are non-randomly occupied. At the treatment temperature of about 570° C, the carbon and nitrogen atoms can easily jump from one site to another and ordered domains, separated by antiphase boundaries, are formed during the cooling. These boundaries can be considered as stacking faults. The fault vector, **R**, which describes the interstitial atom shift is one of the three vectors $\frac{1}{3}\langle 1\,0\,\bar{1}\,0\rangle_{\epsilon_{a\sqrt{3}}}$. The antiphase boundaries are in contrast under two-beam kinematic conditions when the product $\mathbf{g}_{hkil} \cdot \mathbf{R}$ is not an integer where g_{hkil} is the

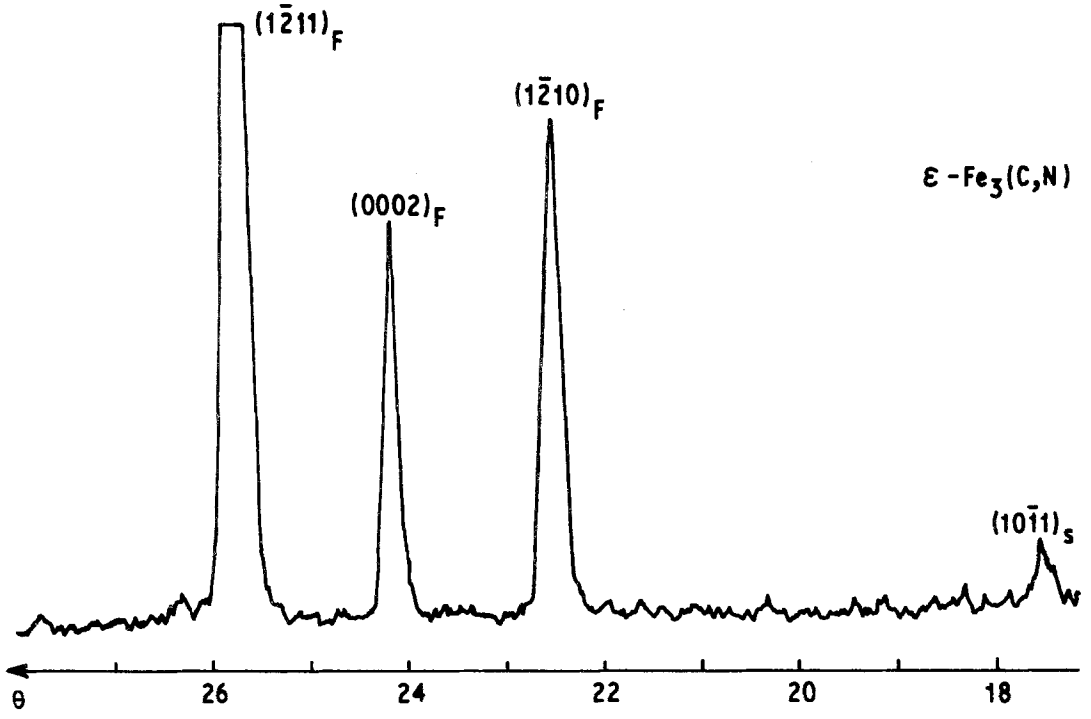

Figure 1 X-ray diffraction pattern of ε-Fe_3(C, N) carbonitride. Extra reflection, S, and fundamental reflections, F, are interpreted using a hexagonal unit cell, $\epsilon_{a\sqrt{3}}$, with parameters $a' = a\sqrt{3}$ and $c' = c$ (a and c being the parameters of the hexagonal close-packed lattice of the iron atoms).

diffracted beam, as a result of which only the superlattice reflections can produce a contrast. The two complementary dark- and bright-field images using a $(10\bar{1}1)_{\epsilon_{a\sqrt{3}}}$ reflection are given as an example in Fig. 2.

3.1.2. Distribution of interstitial atoms in the octahedral sites

Mössbauer spectroscopy was used to study possible ordering between carbon and nitrogen atoms in the octahedral interstitial sites. Two samples of composition $Fe_3(C_{0.32}N_{0.68})$ and $Fe_{3.02}(C_{0.39}N_{0.61})$ were examined. The comparison between the hyperfine parameters of these ε-carbonitrides with those of nitrides having the same interstitial compositions [7] shows that the distribution of the interstitials is non-random. An iron atom is more often in an environment with a carbon and a nitrogen nearest atoms than with either two nitrogen or two carbon nearest atoms.

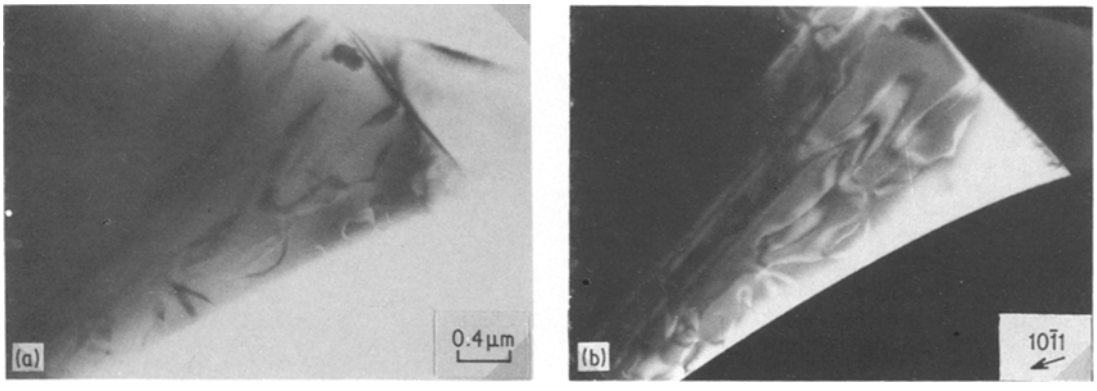

Figure 2 (a) Bright field image of antiphase boundaries in an ε-Fe_3(C, N) crystal. (b) Dark field image using a $1\,0\,\bar{1}\,1_{\epsilon_{a\sqrt{3}}}$ superlattice reflection. The contrast of the domains is reversed.

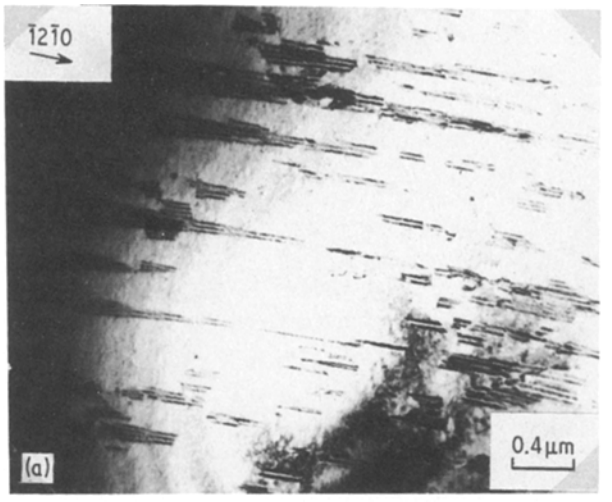

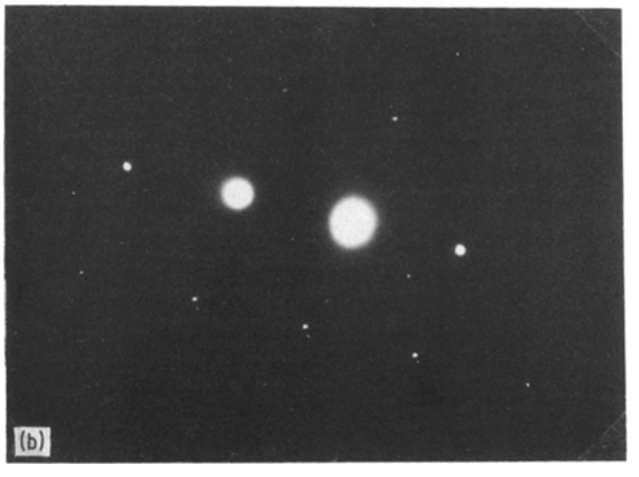

Figure 3 (a) Stacking faults in an ϵ-$Fe_4(C, N)$ crystal carbonitrided at 720° C and quenched. (b) Corresponding electron diffraction pattern with $[\bar{1}\,0\,1\,1]$ zone-axis showing elongated spots in the directions $[1\,0\,2]^*$.

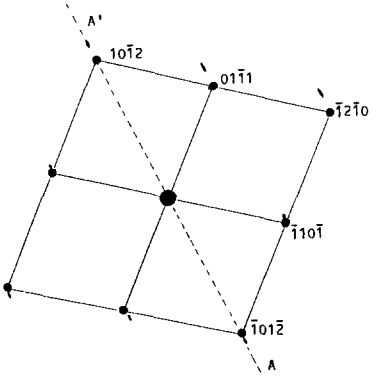

3.2. ϵ-$Fe_4(C, N)$ iron–carbonitride

3.2.1. Crystalline defects

3.2.1.1. Stacking faults. ϵ-carbonitride with stoichiometric formula $Fe_{3.85}(C_{0.18}N_{0.82})$ (near $Fe_4(C, N)$) is formed at a temperature higher than 640° C. It remains unchanged after a drastic quench to room temperature and is seen by electron microscopy to have numerous stacking faults which either cross the crystals or are bounded by two partial dislocations (see Fig. 3).

Trace analyses indicate that the fault plane is the lattice plane (0 0 0 1); this is the usual fault plane of hexagonally close-packed structures.

The fault vector, **R**, was determined by image contrast experiments using two-beam kinematic conditions. According to this method faults become invisible when $\mathbf{g} \cdot \mathbf{R}$ equals an integer. This condition is verified on the micrographs in Fig. 4c and e, formed with the diffracted beams $\mathbf{g}_{2\bar{1}\bar{1}2}$ and $\mathbf{g}_{\bar{1}\bar{1}20}$; this condition is not met on the micrograph in Fig. 4b, formed with the diffracted beam $\mathbf{g}_{0\bar{1}1\bar{1}}$, and the fault can be seen. The corresponding values of the products $\mathbf{g} \cdot \mathbf{R}$ given in Table II, indicate that the fault vector, **R**, is one of the three equivalent vectors $\frac{1}{3}[1\,\bar{1}\,0\,0]$, $\frac{1}{3}[1\,0\,\bar{1}\,0]$ or $\frac{1}{3}[0\,1\,\bar{1}\,0]$. Since these vectors are contained in the close-packed planes of the h c p unit cell, they are located in the fault plane.

Two complementary observations confirm these previous results:

(a) ϵ-carbonitride grains often contain Weiss

TABLE II Values of $\mathbf{g} \cdot \mathbf{R}$ for the stacking faults observed on Fig. 4

Diffracted X-ray beam vector, g	Fault vector, R		
	$\frac{1}{3}[1\,0\,\bar{1}\,0]$	$\frac{1}{3}[1\,\bar{1}\,0\,0]$	$\frac{1}{3}[0\,\bar{1}\,1\,0]$
$0\,\bar{1}\,1\,\bar{1}$	$-\frac{1}{3}$	$\frac{1}{3}$	$\frac{2}{3}$
$2\,\bar{1}\,\bar{1}\,2$	1	1	0
$\bar{1}\,\bar{1}\,2\,0$	-1	0	1

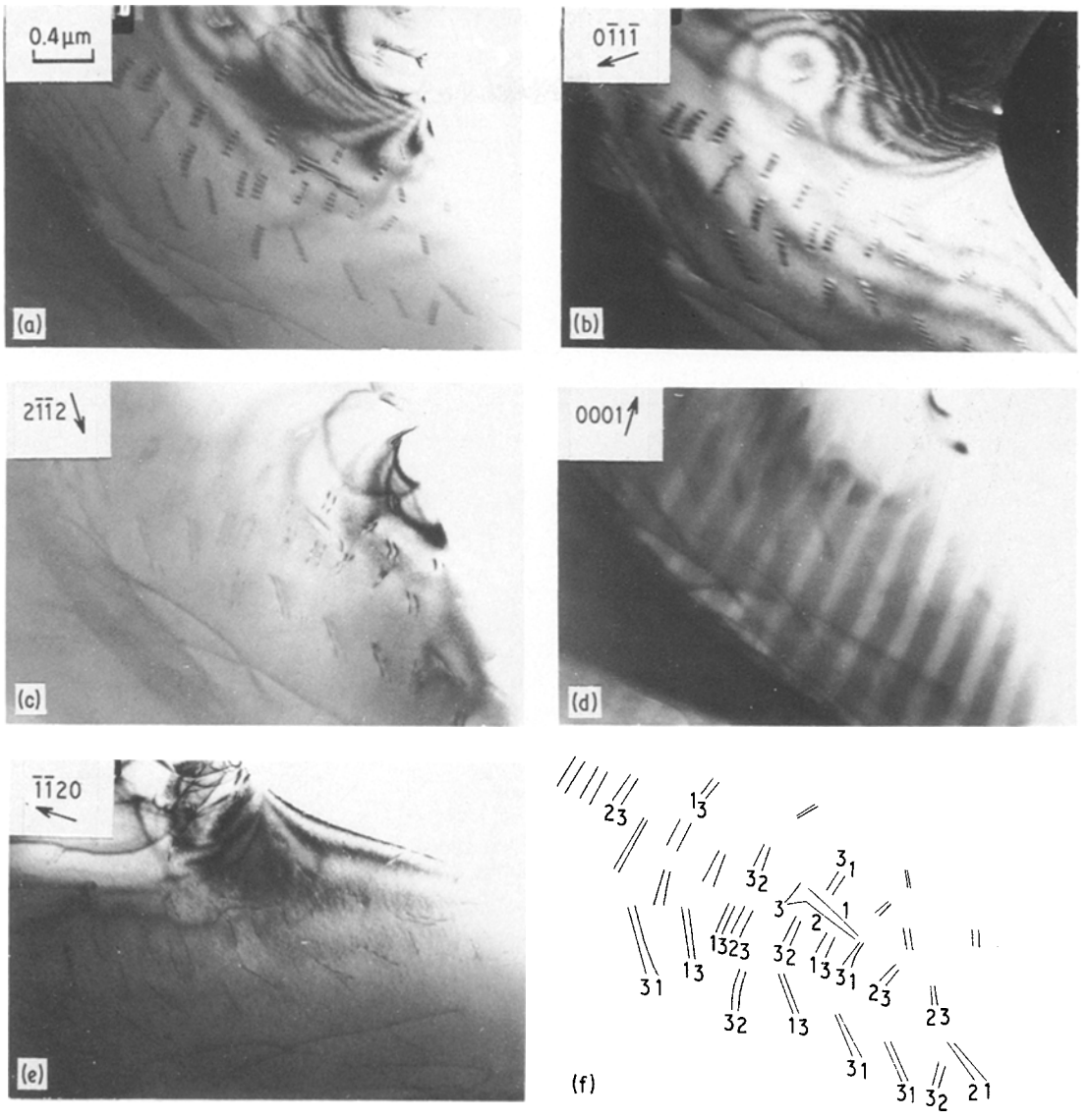

Figure 4 (a) Bright field image of stacking faults and partial dislocations in contrast in an ϵ-$Fe_4(C, N)$ crystal. (b) Corresponding dark field image using a $0\,\bar{1}\,1\,\bar{1}$ reflection. (c) Stacking faults with zero contrast and partial dislocations in contrast; bright field image with $\mathbf{g} = 2\,\bar{1}\,\bar{1}\,2$. (d) Magnetic domains parallel to the direction [0 0 0 1] revealed by using a component of the direct beam. (e) Stacking faults and partial dislocations with zero contrast; bright field image with $\mathbf{g} = \bar{1}\,\bar{1}\,20$. (f) Diagram giving the Burgers vector of some of the partial dislocations: (1) $\mathbf{b} = \frac{1}{3}[1\,0\,\bar{1}\,0]$; (2) $\mathbf{b} = \frac{1}{3}[0\,1\,\bar{1}\,0]$; (3) $\mathbf{b} = \frac{1}{3}[1\,\bar{1}\,0\,0]$.

magnetic domains with their walls parallel to the [0 0 0 1] directions. On the electron micrograph in Fig. 4d, the traces of these walls are perpendicular to the black and white fringes due to the stacking faults with fault plane (0 0 0 1).

(b) Very thin stacking faults produce streaks in the reciprocal lattice which are perpendicular to the fault planes. These streaks are also responsible for the presence of additional spots which are sometimes observed on some diffraction patterns as the thinness of the foil creates an elongation of all the reciprocal lattice nodes over and above the effect due to the stacking faults. The streaks and elongations crossing the same node usually have different elongations and can, depending on the orientation of the foil and the faults, cut the Ewald sphere at two points leading to the formation of two distinct reflections. This effect is observed on the Laüe zone [$\bar{1}$ 0 1 1] given in Fig. 3. The additional spots are directed along $\vec{S}^{x}_{102}$ but trace analysis indicates that elongation is in fact parallel to $\vec{S}^{x}_{001}$ and indicated that the fault planes are (0 0 0 1) planes.

TABLE III Values of $\mathbf{g} \cdot \mathbf{b}$ for the partial dislocations shown in Fig. 4

Diffracted X-ray beam vector, g	Burger's vector, b		
	$\frac{1}{3}[1\,0\,\bar{1}\,0]$ (Labelled 1 in Fig. 4f.)	$\frac{1}{3}[0\,1\,\bar{1}\,0]$ (Labelled 2 in Fig. 4f.)	$\frac{1}{3}[1\,\bar{1}\,0\,0]$ (Labelled 3 in Fig. 4f.)
$0\,\bar{1}\,1\,\bar{1}$	$-\frac{1}{3}$	$-\frac{2}{3}$	$\frac{1}{3}$
$2\,\bar{1}\,\bar{1}\,2$	1	0	1
$\bar{1}\,\bar{1}\,2\,0$	-1	-1	0

3.2.1.2. Partial dislocations. Two partial dislocations at the edges of a stacking fault are located in the fault plane and the sum of their Burgers vectors is either zero or a Burgers vector of a perfect dislocation. In a hcp lattice, the glissile partial dislocation Burgers vectors are of the type $\frac{1}{3}\langle 1\,\bar{1}\,0\,0\rangle$ and the sessile partial dislocation Burgers vectors are of the type $\frac{1}{2}\langle 0\,0\,0\,1\rangle$.

Examination of the contrast of partial dislocations in the electron micrographs of Fig. 4, related to the possible values of the product $\mathbf{g} \cdot \mathbf{b}$, indicate that the Burgers vectors are $\frac{1}{3}\langle 1\,0\,\bar{1}\,0\rangle$ (see Table III).

A dislocation remains invisible if the absolute value of its scalar product $\mathbf{g} \cdot \mathbf{b}$ is lower than $\frac{1}{3}$. Therefore, partial dislocations with zero-contrast in the micrograph in Fig. 4e have, according to Table III, Burgers vectors of $\frac{1}{3}[1\,\bar{1}\,0\,0]$. They are indicated by the number 3 in Fig. 4f. These partial dislocations are in contrast in Fig. 4c and weakly in contrast in Fig. 4a. In this latter case, $\mathbf{g} \cdot \mathbf{b} = \frac{1}{3}$. The partial dislocations in contrast in Fig. 4a and e have $\mathbf{b} = \frac{1}{3}[0\,1\,\bar{1}\,0]$ and are indicated by the number 2 in Fig. 4f; they are invisible in Fig. 4c apart from residual contrast. The partial dislocations which are invisible on the micrograph in Fig. 4a and visible on Fig. 4c and e, the Burgers vector is $\frac{1}{3}[1\,0\,\bar{1}\,0]$ and are indicated by the number 1 in Fig. 4f.

These previous observations indicate that, in ϵ-iron–carbonitride, the partial dislocations at the edges of the stacking faults have Burgers vectors of the type $\frac{1}{3}\langle 1\,\bar{1}\,0\,0\rangle$. Since their **b** vectors are located in the fault plane, they are glissile.

3.2.2. Structural transformation of the ϵ-iron–carbonitrides, $Fe_4(C, N)$, during cooling

3.2.2.1. Homogeneous foils. The Fe–C–N ternary phase diagram shows that the vertical line which describes the composition $Fe_{3.85}(C_{0.18}N_{0.82})$ is located inside the three-phase domain $\epsilon + \gamma' + Fe_3C$ for temperatures lower than 650° C. After quenching and quench-aging, this iron–carbonitride is partially decomposed.

A foil, carbonitrided at 650° C and cooled at a rate of 20° C sec^{-1}, gives the X-ray diffraction pattern given in Fig. 5a. This pattern shows the strong reflections on the ϵ-iron–carbonitride $Fe_{3.85}(C, N)$ and also some weak reflections due to both the γ'-iron–carbonitride phase and a second ϵ-iron–carbon nitride phase whose lattice parameters differ slightly from those of ϵ-$Fe_{3.85}(C, N)$. According to the relationships between the lattice parameters and the interstitial atom contents, claimed by Jack [5], it has a probable stoichiometric formula of $Fe_3(C, N)$. None of the reflections of cementite are observed after this fast cooling since the transformation equilibrium is not reached. A cooling rate of 20° C sec^{-1} does not allow the initial carbonitride, $Fe_{3.85}(C, N)$, to be entirely retained at room temperature: it is partially transformed. Transformation can be achieved after ageing. This evolution is studied by comparing the intensities of the reflections of the two ϵ-iron–carbonitrides.

Such a quenched foil, aged for 20 h at a temperature of 200° C, gives X-ray diffraction reflections (see Fig. 5b) the intensities and positions of which have changed in comparison with the initial pattern (Fig. 5a). The reflections of the ϵ-$Fe_3(C, N)$ iron–carbonitride obtained after ageing have stronger intensities, showing that the ϵ-$Fe_{3.85}(C, N)$ formed at high-temperature is almost completely decomposed. The intensities of the reflections of γ'-carbonitride have not been noticeably modified, whereas the expected transformation during the thermal treatment:

$$\epsilon\text{-}Fe_4(C, N)_{hex} \rightarrow \epsilon\text{-}Fe_3(C, N)_{hex} + \gamma'\text{-}Fe_4(C, N)_{cub} + Fe_3C$$

should give γ'-iron–carbonitride and cementite. Detailed observations of these foils, by electron microscopy, show the presence of six families of precipitates, P, containing thin planar defects

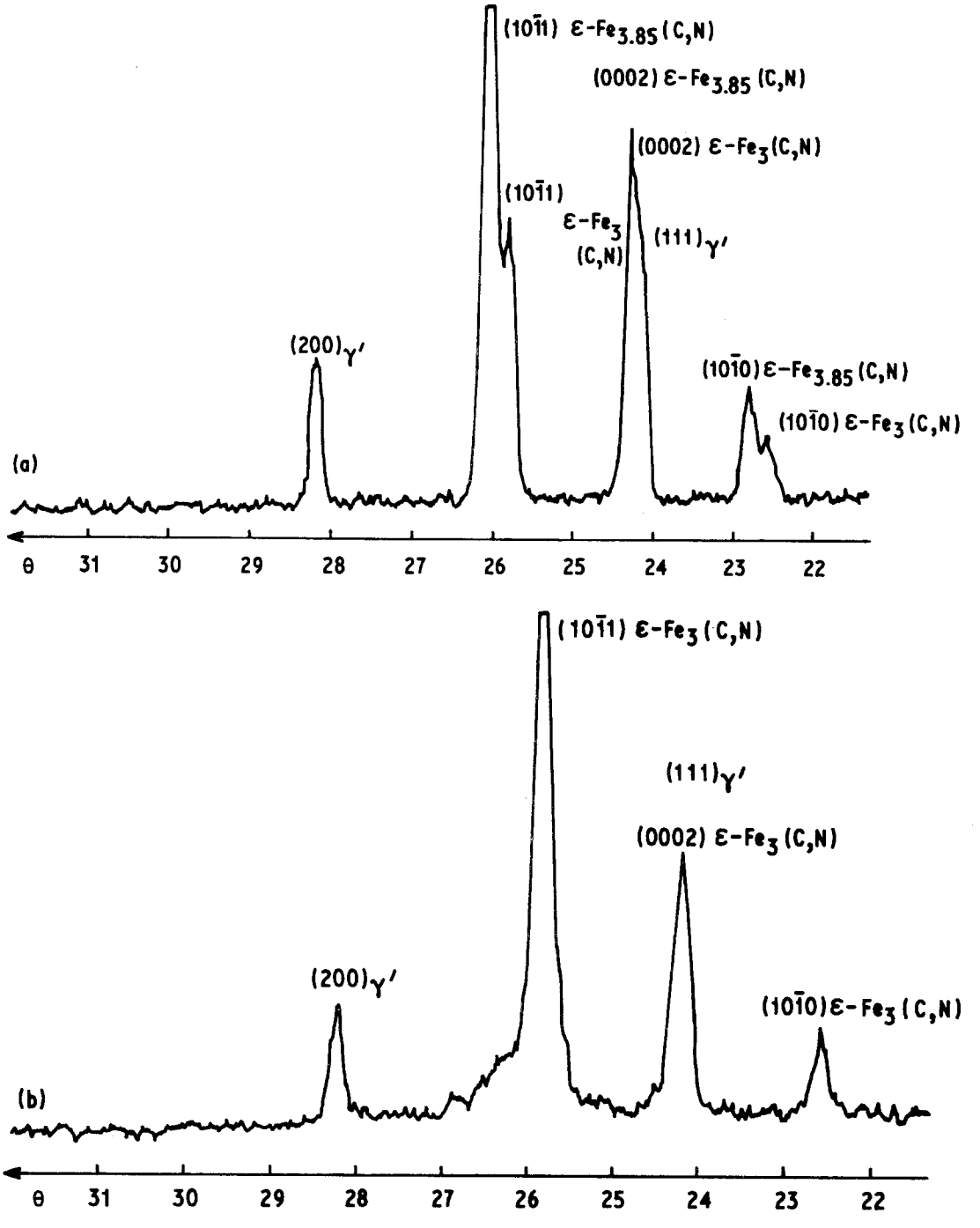

Figure 5 X-ray diffraction pattern obtained with an ϵ-$Fe_{3\cdot85}(C, N)$ foil. (a) Fast cooled after a carbonitriding treatment at 640° C. (b) Aged for 20 h at 200° C. The interstitial content of the ϵ-matrix is increased.

(Fig. 6). Since these precipitates are neither γ'-carbonitride nor cementite, the observed phases do not agree with the above equilibrium relationship; intermediate stages in the decomposition of ϵ-$Fe_4(C, N)$ lead to a metastable precipitation.

The corresponding electron diffraction patterns exhibit, in addition to the reflections due to the matrix, ϵ, and to the precipitates, P, streaks which are perpendicular to the planar defects. Although these streaks prevent the accurate measurement of the *d*-spacings, all the diffraction patterns can be indexed using a body-centred cubic unit cell with

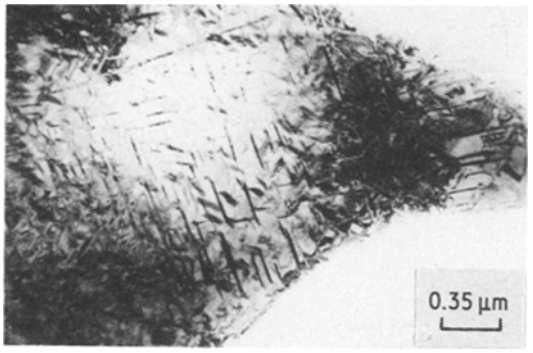

Figure 6 Bright field image of an ϵ-$Fe_{3.85}(C, N)$ grain aged for 20 h at 200° C containing six families of precipitates.

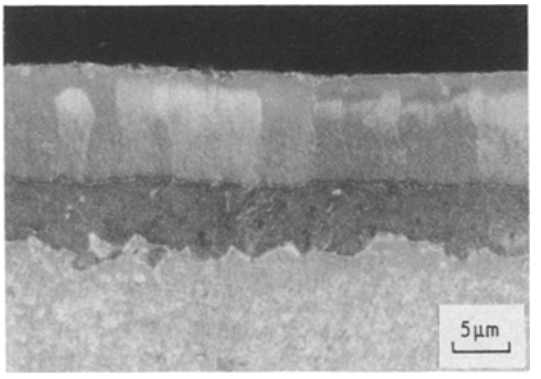

Figure 7 ϵ-iron carbonitride layer followed by an austenite layer formed at the surface of a sample carbonitrided at 600° C.

a parameter, a, of approximately 2.86 Å. Relationships between the precipitates, P, and the matrix, ϵ, are as follows:

$$\{0\,0\,0\,1\}_\epsilon \parallel \{1\,0\,1\}_P$$

$$\langle\bar{2}\,1\,1\,0\rangle_\epsilon \parallel \langle 0\,1\,0\rangle_P.$$

The habit plane is $\{1\,1\,\bar{2}\,2\}_\epsilon$. The interstitial content of the ϵ-matrix increases during ageing, therefore the new phase P is poor in carbon and nitrogen and is likely to be metastable. Over-ageing should lead to the formation of the two equilibrium phases, γ' and Fe_3C. The precipitates have a very small size and, for that reason, they do not produce any visible reflections in the X-ray diffraction pattern shown in Fig. 5b.

3.2.2.2. Bulk specimens. Fig. 7 shows the structure of an ϵ-layer obtained on a bulk pure iron sample after ion–carbonitriding at 600° C and quenching. The ϵ-layer is followed by an austenite layer which is unsuitable for some applications. Nevertheless, it will not be formed if the treatment temperature is lowered by 20° C.

(a) Structure after quench-ageing. After quenching, the microhardness of the ϵ-layer is approximately 750 VHN regardless of layer thickness. Sequential transformations occur in the ϵ-layer after slow cooling or quench-ageing which are due both to the existence of gradients in the carbon and nitrogen concentrations in layers obtained by a diffusion mechanism, and also to modifications of the ϵ-iron–carbonitride equilibrium domain with changing temperature.

Fig. 8 shows, for some ageing temperatures, a plot of the maximum microhardness in the ϵ-layer against the ageing time. At 500° C the hardness is approximately 800 VHN and is constant for all layer thicknesses.

At 400° C and 300° C, the maximum hardness reaches 1200 and 1300 VHN, respectively, after one hour of ageing. In these cases, softening is due to the precipitation of γ'-iron–carbonitride. At 200° C, the maximum microhardness is constant during a two hour incubation period but then rises to 1600 VHN after ageing for longer than 64 hours. This particular behaviour, and the observations by electron microscopy of small precipitates after ageing at 200° C, characterize a structural hardening. The stability of the metastable precipitates seems to be great enough for them to have industrial applications. It could be particularly useful in the ion carbonitriding of low-alloy steels which should have good resistance to mechanical abrasion and wear. Strengthening may also occur during the use of carbonitrided mechanical parts. To benefit from this precipitation-hardening, the diffusion treatment must be followed by a quench; otherwise, the properties of the ϵ-layer are quite different.

(b) Structure after slow cooling and ageing. According to the ternary Fe–C–N phase diagram, the layer, after slow cooling to room temperature, is composed of:

(a) a matrix of hexagonal ϵ-iron–carbonitride whose interstitial content is approximately 25 at %;

(b) γ'-carbonitride $Fe_4(C, N)$ precipitates;

(c) a small amount of cementite Fe_3C precipitates;

(d) precipitates of ferrite which occasionally appear when the treatment is performed at a temperature higher than 570° C.

Precipitates of ϵ- and γ'-phases are in the shape

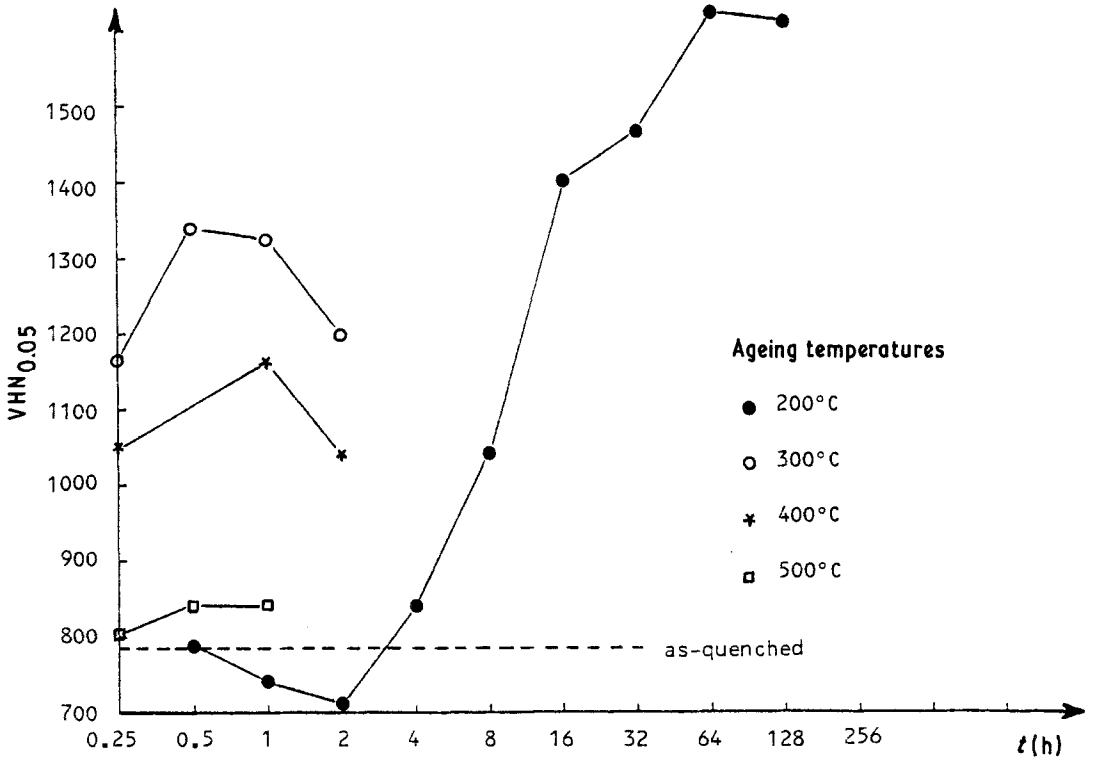

Figure 8 The effect of ageing time on the maximum microhardness in ϵ-layers.

of thin plates whose faces are, respectively, parallel to the $(0\,0\,0\,1)_\epsilon$ and $(1\,1\,1)_{\gamma'}$ directions (see Fig. 9).

Two twinned families of γ'-carbon nitride with twinning planes $\{1\,1\,1\}_\gamma$ are often observed. Electron diffraction patterns allow the following relationships [8] to be defined:

$$\{0\,0\,0\,1\}_\epsilon \parallel \{1\,1\,1\}_{\gamma'} \parallel \{1\,0\,1\}_\alpha;$$

$$\langle\bar{2}\,1\,1\,0\rangle_\epsilon \parallel \langle 1\,\bar{1}\,0\rangle_{\gamma'} \parallel \langle 1\,1\,\bar{1}\rangle_\alpha \text{ or } \langle 0\,1\,0\rangle_\alpha.$$

These relationships are also observed in the two-phase samples $\epsilon + \gamma'$ or $\gamma' + \alpha$ obtained by homogeneous carbonitriding and quenching of iron foils. Thus, they cannot be linked to the cooling rate of the ϵ-layer.

3.2.3. A model of ϵ-phase–γ'-phase transformation during cooling

These previous observations allow a model, representing the transformation from the hexagonal ϵ-phase to the cubic γ'-phase, to be proposed.

X-ray lattice parameter measurements of the hexagonal phase, ϵ-$Fe_4(C, N)$, indicate that the ratio c/a is very nearly equal to $\sqrt{8/3}$ and, therefore, that the iron atom lattice has a true hexagonal close-packed unit cell. By analogy with the allotropic transformation $\alpha \rightleftarrows \beta$ of cobalt [9–11] a f c c ϵ-type with parameters $a_{fcc} = a_{hcp}\sqrt{2}$ can be expected. If the interstitial atoms are not taken into account, the lattice parameters and the unit-cell of the γ'-phase verify these conditions. According to this model, the change from $\epsilon \rightarrow \gamma'_x$ is brought about by the slips of the $(0\,0\,0\,1)$ iron atom planes by means of partial dislocations of type $\frac{1}{3}\langle 1\,0\,\bar{1}\,0\rangle_\epsilon$ [12].

If the hexagonal crystal is shifted by a translation of $\frac{1}{3}\langle 1\,0\,\bar{1}\,0\rangle$ successively in every basal plane, the h c p structure is fully changes into a f c c structure. If the slip occurs sometimes in two successive close-packed planes, the stacking sequence obtained represents a twinned f c c structure with a $(1\,1\,1)$ twinning plane. This particular mechanism agrees with the observations of two twinned families of γ'-iron–carbonitride.

4. Conclusions

A microstructural study of ϵ-iron–carbonitrides formed by ion-bombardment has been carried out on both homogeneous foils and bulk samples of pure iron.

Detailed observations of superlattice reflections

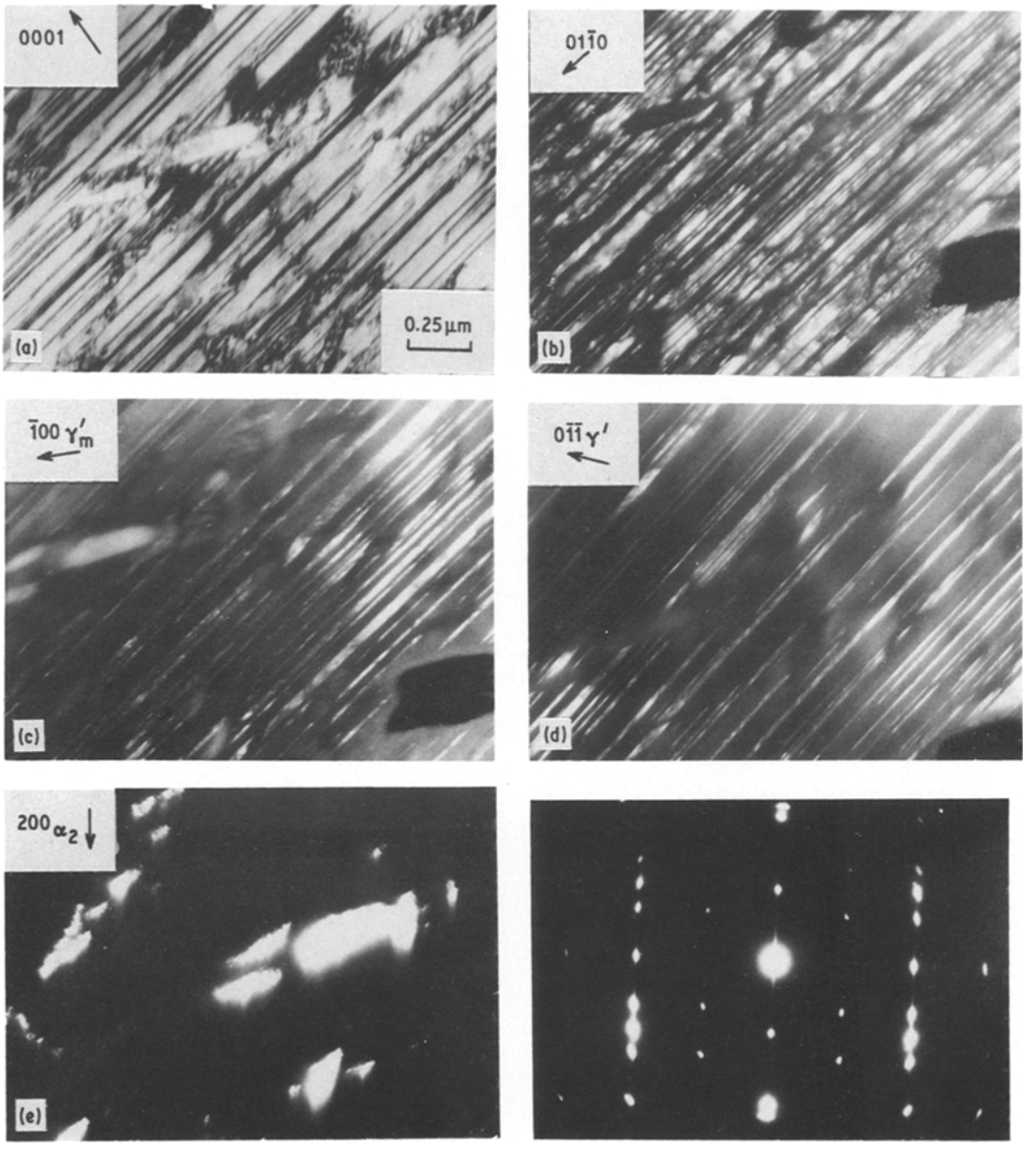

Figure 9 (a) Bright field image showing an ϵ-iron–carbonitride grain located in the vicinity of the interface ϵ–γ'. (b–e) Dark field images using $0\,1\,\bar{1}\,0_\epsilon$, $\bar{1}\,0\,0_{\gamma' m}$, $0\,\bar{1}\,\bar{1}_{\gamma'}$ and $2\,0\,0_{\alpha_2}$ reflections. (f) Electron diffraction pattern corresponding to the micrograph in (a).

encountered on X-ray and electron diffraction patterns indicated some ordering of interstitial atoms in ϵ-iron–carbonitride within the composition range $Fe_3(C, N)$. The interstitial atoms have a hexagonal lattice with parameters $a' = a\sqrt{3}$ and $c' = c$, where a and c are the parameters of the hexagonal close-packed iron lattices.

Evidence of this order is supported by obser-

vations of antiphase domains using electron microscopy. Mössbauer spectrometry indicates that each iron atom is more likely to be surrounded by a carbon and a nitrogen atom than by either two nitrogen or two carbon atoms.

ϵ-iron–carbonitride, with an interstitial content of approximately 20 at %, shows, after quenching, many stacking faults with (0001) fault planes. Partial dislocations with Burgers vectors $\mathbf{b} = \frac{1}{3}\langle 1\,0\,\bar{1}\,0\rangle$ are encountered at the edges of the stacking faults.

Low interstitial content ϵ-layers can be strengthened by a fine precipitation after quenching at low temperatures; six families of metastable precipitates with low interstitial content are usually observed.

After slow cooling, ϵ-carbon nitride, γ'-carbon nitride and ferrite occur simultaneously in ϵ-phase crystal with the following relationships:

$$\{0\,0\,0\,1\}_\epsilon \parallel \{1\,1\,1\}_{\gamma'} \parallel \{1\,0\,1\}_\alpha;$$

$$\langle\bar{2}\,1\,1\,0\rangle_\epsilon \parallel \langle 1\,\bar{1}\,0\rangle_{\gamma'} \parallel \langle 1\,1\,\bar{1}\rangle_\alpha \text{ or } \langle 0\,1\,0\rangle_\alpha.$$

From these observations, a model of transformation of ϵ-Fe_4N to γ'-Fe_4N is proposed. It takes into account slips of the basal planes formed by the iron atoms through displacements of partial dislocations with Burgers vector $\frac{1}{3}\langle 1\,0\,\bar{1}\,0\rangle$.

References

1. J. P. LEBRUN, H. MICHEL and M. GANTOIS, *Memoirs Sci. Rev. Met.* **69** (1972) 727.
2. F. HOMBECK and B. EDENHOFER, Proceedings of the International Conference on Physical Metallurgy Aspects of Surface Coatings (The Iron and Steel Institute, London, 1973).
3. C. K. JONES, S. W. MARTIN, D. J. STURGES and M. HUDIS, Proceedings of the Heat Treatment '73 Conference, December 1973, London (The Metal Society, London, 1975).
4. R. BERNERON, J. MANENC, H. MICHEL and M. GANTOIS, *Memoirs Sci. Rev. Met.* **76** (1979) 109.
5. K. H. JACK, *Acta. Cryst.* **5** (1952) 404.
6. J. B. HENDRICKS and P. B. KOSTING, *Z. Kryst.* **74** (1930) 511.
7. F. FOCT, *J. de Physique* **35 C6** (1974) 487.
8. D. GERARDIN, H. MICHEL and M. GANTOIS, *Scripta Met.* **11** (1977) 557.
9. J. W. CHRISTIAN, *Proc. Roy. Soc.* **206A** (1951) 51.
10. H. BIBRING and F. SEBILLEAU, *Rev. Met.* **52** (1955) 569.
11. A. SEEGER, *Z. Metallkunde* **47** (1956) 653.
12. D. GERARDIN, H. MICHEL, J. P. MORNIROLI and M. GANTOIS, *Memoirs Sci. Rev. Met.* **74** (1977) 457.
13. F. C. FRANK and J. F. NICHOLAS, *Phil. Mag.* **44** (1953) 358, 1213.

Received 3 January and accepted 30 June 1980.